# Measurement of $D^{*\pm}$ meson production in $e^{\pm}p$ scattering at low Q^2

ZEUS Collaboration

Abstract

The production of $D^{*\pm}(2010)$ mesons in $e^{\pm}p$ scattering in the range of exchanged photon virtuality $0.05 < Q^2 < 0.7 \, \mathrm{GeV}^2$ has been measured with the ZEUS detector at HERA using an integrated luminosity of 82 pb^{-1}. The decay channels $D^{*+} \to D^0\pi^+$ with $D^0 \to K^-\pi^+$ and corresponding antiparticle decay were used to identify D^* mesons and the ZEUS beampipe calorimeter was used to identify the scattered electron. Differential D^* cross sections as functions of Q^2, inelasticity, y, transverse momentum of the D^* meson, $p_T(D^*)$, and pseudorapidity of the D^* meson, $\eta(D^*)$, have been measured in the kinematic region $0.02 < y < 0.85$, $1.5 < p_T(D^*) < 9.0 \, \mathrm{GeV}$ and $|\eta(D^*)| < 1.5$. The measured differential cross sections are in agreement with two different NLO QCD calculations. The cross sections are also compared to previous ZEUS measurements in the photoproduction and DIS regimes.
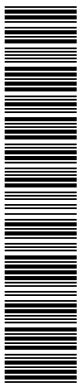
The ZEUS Collaboration

S. Chekanov[1], M. Derrick, S. Magill, S. Miglioranzi[2], B. Musgrave, D. Nicholass[2], J. Repond, R. Yoshida
Argonne National Laboratory, Argonne, Illinois 60439-4815, USA [n]

M.C.K. Mattingly
Andrews University, Berrien Springs, Michigan 49104-0380, USA

M. Jechow, N. Pavel [†], A.G. Yagües Molina
Institut für Physik der Humboldt-Universität zu Berlin, Berlin, Germany

S. Antonelli, P. Antonioli, G. Bari, M. Basile, L. Bellagamba, M. Bindi, D. Boscherini, A. Bruni, G. Bruni, L. Cifarelli, F. Cindolo, A. Contin, M. Corradi[3], S. De Pasquale, G. Iacobucci, A. Margotti, R. Nania, A. Polini, L. Rinaldi, G. Sartorelli, A. Zichichi
University and INFN Bologna, Bologna, Italy [e]

D. Bartsch, I. Brock, S. Goers[4], H. Hartmann, E. Hilger, P. Irrgang[5], H.-P. Jakob, M. Jüngst, O.M. Kind, E. Paul[6], R. Renner, U. Samson, V. Schönberg, R. Shehzadi, M. Wlasenko
Physikalisches Institut der Universität Bonn, Bonn, Germany [b]

N.H. Brook, G.P. Heath, J.D. Morris, T. Namsoo
H.H. Wills Physics Laboratory, University of Bristol, Bristol, United Kingdom [m]

M. Capua, S. Fazio, A. Mastroberardino, M. Schioppa, G. Susinno, E. Tassi
Calabria University, Physics Department and INFN, Cosenza, Italy [e]

J.Y. Kim[7], K.J. Ma[8]
Chonnam National University, Kwangju, South Korea [g]

Z.A. Ibrahim, B. Kamaluddin, W.A.T. Wan Abdullah
Jabatan Fizik, Universiti Malaya, 50603 Kuala Lumpur, Malaysia [r]

Y. Ning, Z. Ren, F. Sciulli
Nevis Laboratories, Columbia University, Irvington on Hudson, New York 10027 [o]

J. Chwastowski, A. Eskreys, J. Figiel, A. Galas, M. Gil, K. Olkiewicz, P. Stopa, L. Zawiejski
The Henryk Niewodniczanski Institute of Nuclear Physics, Polish Academy of Sciences, Cracow, Poland [i]

L. Adamczyk, T. Bołd, I. Grabowska-Bołd, D. Kisielewska, J. Łukasik, M. Przybycień, L. Suszycki
Faculty of Physics and Applied Computer Science, AGH-University of Science and Technology, Cracow, Poland [p]

A. Kotański[9], W. Słomiński
Department of Physics, Jagellonian University, Cracow, Poland

V. Adler, U. Behrens, I. Bloch, C. Blohm, A. Bonato, K. Borras, N. Coppola, A. Dossanov, J. Fourletova, A. Geiser, D. Gladkov, P. Göttlicher[10], I. Gregor, T. Haas, W. Hain, C. Horn, B. Kahle, U. Klein[11], U. Kötz, H. Kowalski, E. Lobodzinska, B. Löhr, R. Mankel, I.-A. Melzer-Pellmann, A. Montanari, D. Notz, A.E. Nuncio-Quiroz, I. Rubinsky, R. Santamarta, U. Schneekloth, A. Spiridonov[12], H. Stadie, D. Szuba[13], J. Szuba[14], T. Theedt, G. Wolf, K. Wrona, C. Youngman, W. Zeuner
Deutsches Elektronen-Synchrotron DESY, Hamburg, Germany

W. Lohmann, S. Schlenstedt
Deutsches Elektronen-Synchrotron DESY, Zeuthen, Germany

G. Barbagli, E. Gallo, P. G. Pelfer
University and INFN, Florence, Italy [e]

A. Bamberger, D. Dobur, F. Karstens, N.N. Vlasov[15]
Fakultät für Physik der Universität Freiburg i.Br., Freiburg i.Br., Germany [b]

P.J. Bussey, A.T. Doyle, W. Dunne, J. Ferrando, D.H. Saxon, I.O. Skillicorn
Department of Physics and Astronomy, University of Glasgow, Glasgow, United Kingdom [m]

I. Gialas[16]
Department of Engineering in Management and Finance, Univ. of Aegean, Greece

T. Gosau, U. Holm, R. Klanner, E. Lohrmann, H. Salehi, P. Schleper, T. Schörner-Sadenius, J. Sztuk, K. Wichmann, K. Wick
Hamburg University, Institute of Exp. Physics, Hamburg, Germany [b]

C. Foudas, C. Fry, K.R. Long, A.D. Tapper
Imperial College London, High Energy Nuclear Physics Group, London, United Kingdom [m]

M. Kataoka[17], T. Matsumoto, K. Nagano, K. Tokushuku[18], S. Yamada, Y. Yamazaki
Institute of Particle and Nuclear Studies, KEK, Tsukuba, Japan [f]

A.N. Barakbaev, E.G. Boos, N.S. Pokrovskiy, B.O. Zhautykov
Institute of Physics and Technology of Ministry of Education and Science of Kazakhstan, Almaty, Kazakhstan

D. Son
Kyungpook National University, Center for High Energy Physics, Daegu, South Korea [g]

J. de Favereau, K. Piotrzkowski
Institut de Physique Nucléaire, Université Catholique de Louvain, Louvain-la-Neuve, Belgium [q]

F. Barreiro, C. Glasman[19], M. Jimenez, L. Labarga, J. del Peso, E. Ron, M. Soares, J. Terrón, M. Zambrana
Departamento de Física Teórica, Universidad Autónoma de Madrid, Madrid, Spain [l]

F. Corriveau, C. Liu, R. Walsh, C. Zhou
Department of Physics, McGill University, Montréal, Québec, Canada H3A 2T8 [a]

T. Tsurugai
Meiji Gakuin University, Faculty of General Education, Yokohama, Japan [f]

A. Antonov, B.A. Dolgoshein, V. Sosnovtsev, A. Stifutkin, S. Suchkov
Moscow Engineering Physics Institute, Moscow, Russia [j]

R.K. Dementiev, P.F. Ermolov, L.K. Gladilin, I.I. Katkov, L.A. Khein, I.A. Korzhavina, V.A. Kuzmin, B.B. Levchenko[20], O.Yu. Lukina, A.S. Proskuryakov, L.M. Shcheglova, D.S. Zotkin, S.A. Zotkin
Moscow State University, Institute of Nuclear Physics, Moscow, Russia [k]

I. Abt, C. Büttner, A. Caldwell, D. Kollar, W.B. Schmidke, J. Sutiak
Max-Planck-Institut für Physik, München, Germany

G. Grigorescu, A. Keramidas, E. Koffeman, P. Kooijman, A. Pellegrino, H. Tiecke, M. Vázquez[17], L. Wiggers
NIKHEF and University of Amsterdam, Amsterdam, Netherlands [h]

N. Brümmer, B. Bylsma, L.S. Durkin, A. Lee, T.Y. Ling
Physics Department, Ohio State University, Columbus, Ohio 43210 [n]

P.D. Allfrey, M.A. Bell, A.M. Cooper-Sarkar, A. Cottrell, R.C.E. Devenish, B. Foster, K. Korcsak-Gorzo, S. Patel, V. Roberfroid[21], A. Robertson, P.B. Straub, C. Uribe-Estrada, R. Walczak
Department of Physics, University of Oxford, Oxford United Kingdom [m]

P. Bellan, A. Bertolin, R. Brugnera, R. Carlin, R. Ciesielski, F. Dal Corso, S. Dusini, A. Garfagnini, S. Limentani, A. Longhin, L. Stanco, M. Turcato
Dipartimento di Fisica dell' Università and INFN, Padova, Italy [e]

B.Y. Oh, A. Raval, J. Ukleja[22], J.J. Whitmore[23]
Department of Physics, Pennsylvania State University, University Park, Pennsylvania 16802 [o]

Y. Iga
Polytechnic University, Sagamihara, Japan [f]

G. D'Agostini, G. Marini, A. Nigro

Dipartimento di Fisica, Università 'La Sapienza' and INFN, Rome, Italy [e]

J.E. Cole, J.C. Hart

Rutherford Appleton Laboratory, Chilton, Didcot, Oxon, United Kingdom [m]

H. Abramowicz[24], A. Gabareen, R. Ingbir, S. Kananov, A. Levy

Raymond and Beverly Sackler Faculty of Exact Sciences, School of Physics, Tel-Aviv University, Tel-Aviv, Israel [d]

M. Kuze

Department of Physics, Tokyo Institute of Technology, Tokyo, Japan [f]

R. Hori, S. Kagawa[25], N. Okazaki, S. Shimizu, T. Tawara

Department of Physics, University of Tokyo, Tokyo, Japan [f]

R. Hamatsu, H. Kaji[26], S. Kitamura[27], O. Ota, Y.D. Ri

Tokyo Metropolitan University, Department of Physics, Tokyo, Japan [f]

M.I. Ferrero, V. Monaco, R. Sacchi, A. Solano

Università di Torino and INFN, Torino, Italy [e]

M. Arneodo, M. Ruspa

Università del Piemonte Orientale, Novara, and INFN, Torino, Italy [e]

S. Fourletov, J.F. Martin

Department of Physics, University of Toronto, Toronto, Ontario, Canada M5S 1A7 [a]

S.K. Boutle[16], J.M. Butterworth, C. Gwenlan[28], R. Hall-Wilton[17], T.W. Jones, J.H. Loizides, M.R. Sutton[28], C. Targett-Adams, M. Wing

Physics and Astronomy Department, University College London, London, United Kingdom [m]

B. Brzozowska, J. Ciborowski[29], G. Grzelak, P. Kulinski, P. Łużniak[30], J. Malka[30], R.J. Nowak, J.M. Pawlak, T. Tymieniecka, A. Ukleja[31], A.F. Żarnecki

Warsaw University, Institute of Experimental Physics, Warsaw, Poland

M. Adamus, P. Plucinski[32]

Institute for Nuclear Studies, Warsaw, Poland

Y. Eisenberg, I. Giller, D. Hochman, U. Karshon, M. Rosin

Department of Particle Physics, Weizmann Institute, Rehovot, Israel [c]

E. Brownson, T. Danielson, A. Everett, D. Kçira, D.D. Reeder[6], P. Ryan, A.A. Savin, W.H. Smith, H. Wolfe

Department of Physics, University of Wisconsin, Madison, Wisconsin 53706, USA [n]

S. Bhadra, C.D. Catterall, Y. Cui, G. Hartner, S. Menary, U. Noor, J. Standage, J. Whyte

Department of Physics, York University, Ontario, Canada M3J 1P3 [a]

1 Introduction

The production of charm quarks at HERA has been studied both in deep inelastic scattering (DIS) [1–5] and photoproduction [6–10]. In general, reasonable agreement is seen with next-to-leading-order (NLO) QCD predictions.

This paper presents measurements of the D^* cross section in the range $0.05 < Q^2 < 0.7\,\mathrm{GeV}^2$. The beampipe calorimeter of ZEUS [11,12] was used for the measurement of the scattered lepton, which allows the first measurements of the transition region between photoproduction (photon virtuality, $Q^2 \sim 0\,\mathrm{GeV}^2$) and DIS ($Q^2 > 1\,\mathrm{GeV}^2$). The cross sections are compared to the predictions of two different NLO QCD calculations, one designed for DIS, the other for the photoproduction region. This paper investigates whether the calculations remain valid in this transition region.

2 Experimental set-up

This analysis was performed with data taken from 1998 to 2000, when HERA collided electrons or positrons[1] with energy $E_e = 27.5\,\mathrm{GeV}$ with protons of energy $E_p = 920\,\mathrm{GeV}$. The combined data sample has an integrated luminosity of $\mathcal{L} = 81.9 \pm 1.8\,\mathrm{pb}^{-1}$.

A detailed description of the ZEUS detector can be found elsewhere [13]. A brief outline of the components that are most relevant for this analysis is given below.

Charged particles are tracked in the central tracking detector (CTD) [14], which operates in a magnetic field of 1.43 T provided by a thin superconducting coil. The CTD consists of 72 cylindrical drift chamber layers, organized in nine superlayers covering the polar-angle[2] region $15° < \theta < 164°$. The transverse-momentum resolution for full-length tracks is $\sigma(p_T)/p_T = 0.0058 p_T \oplus 0.0065 \oplus 0.0014/p_T$, with p_T in GeV.

The high-resolution uranium-scintillator calorimeter (CAL) [15] consists of three parts: the forward (FCAL), the barrel (BCAL) and the rear (RCAL) calorimeters. Each part is subdivided transversely into towers and longitudinally into one electromagnetic section and either one (in RCAL) or two (in BCAL and FCAL) hadronic sections. The smallest subdivision of the calorimeter is called a cell. The CAL energy resolutions, as measured under test-beam conditions, are $\sigma(E)/E = 0.18/\sqrt{E}$ for electrons and $\sigma(E)/E = 0.35/\sqrt{E}$ for hadrons, with E in GeV.

---

[1] Hereafter, both electrons and positrons are referred to as electrons.

[2] The ZEUS coordinate system is a right-handed Cartesian system, with the Z axis pointing in the proton beam direction, referred to as the "forward direction", and the X axis pointing left towards the centre of HERA. The coordinate origin is at the nominal interaction point.

The scattered electron was detected in the beampipe calorimeter (BPC). The BPC allowed the detection of low-Q^2 events, where the electron is scattered through a small angle. The BPC was used in previous measurements of the proton structure function, F_2, at low Q^2 [11,12]. It originally consisted of two tungsten–scintillator sampling calorimeters with the front faces located at $Z = -293.7\,\mathrm{cm}$, the centre at $Y = 0.0\,\mathrm{cm}$, and the inner edge of the active area at $X = \pm 4.4\,\mathrm{cm}$, as close as possible to the electron-beam trajectory. At the end of 1997 one of the two BPC calorimeters was removed; hence, for the analysis in this paper, only the calorimeter located on the $+X$ side of the beampipe was utilised. It had an active area of $12.0 \times 12.8\,\mathrm{cm^2}$ in $X \times Y$ and a depth of 24 radiation lengths. The relative energy resolution as determined in test-beam measurements with $1-6\,\mathrm{GeV}$ electrons was $\Delta E/E = 17\%/\sqrt{E\,(\,\mathrm{GeV})}$.

The luminosity was measured from the rate of the bremsstrahlung process $ep \to e\gamma p$, where the photon was measured in a lead–scintillator calorimeter [16] placed in the HERA tunnel at Z=-107m.

A three-level trigger system was used to select events online [13,17]. At all three levels, the event was required to contain a scattered electron candidate in the BPC. Additionally, at the third level, a reconstructed D^* candidate was required for the event to be kept for further analysis. The efficiency of the online D^* reconstruction, determined relative to an inclusive DIS trigger, was above 95% [5].

3   Kinematic reconstruction and event selection

Deep inelastic electron-proton scattering, $ep \to eX$, can be described in terms of two kinematic variables, chosen here to be y and Q^2, where y is the inelasticity. They are defined as $Q^2 = -q^2 = -(k - k')^2$ and $y = Q^2/(2P \cdot q)$, where k and P are the four-momenta of the incoming electron and proton, respectively, and k' is the four-momentum of the scattered electron. The inelasticity, which is the fractional energy transferred to the proton in its rest frame, is related to the Bjorken scaling variable x and Q^2 by $Q^2 = sxy$, where $s = 4E_eE_p$ is the square of the electron-proton centre-of-mass energy of $318\,\mathrm{GeV}$.

The values of y and Q^2 were calculated using the measured electron scattering angle and the energy deposited in the BPC as detailed in a previous analysis [11], which also describes the method used for the energy calibration of the BPC. A time dependent re-calibration of the energy response was necessary [18], as radiation damage of the scintillator resulted in a degradation of about 10% by the end of the 2000 running period.

A series of cuts was applied to reject background. The events were required to have a primary vertex within $50\,\mathrm{cm}$ in Z of the nominal interaction point. The electron candidates in the BPC were required to have $E_{\mathrm{BPC}} > 4\,\mathrm{GeV}$, as the trigger efficiency is low below this

energy. The electron impact point on the face of the BPC was required to be more than $0.7\,\mathrm{cm}$ from the inner edge to ensure good shower containment. Photoproduction events were efficiently rejected by requiring the events to have $35 < E - P_Z < 65\,\mathrm{GeV}$, where $E - P_Z = \sum_i (E - P_Z)_i$ is summed over all CAL deposits, including the scattered electron candidate in the BPC. Finally, events with an additional well-reconstructed electron candidate in the CAL with energy greater than $5\,\mathrm{GeV}$ were rejected to reduce background from DIS events with $Q^2 > 1\,\mathrm{GeV}^2$.

The measured kinematic region in y and Q^2 was restricted to the range of high acceptance, $0.02 < y < 0.85$, $0.05 < Q^2 < 0.7\,\mathrm{GeV}^2$. With these cuts, the reconstructed invariant mass of the hadronic system, W, lies between 50 and $300\,\mathrm{GeV}$, with a mean of $190\,\mathrm{GeV}$.

4 Selection of D^* candidates

The D^* mesons were identified using the decay channel $D^{*+} \to D^0 \pi_s^+$ with the subsequent decay $D^0 \to K^- \pi^+$ and the corresponding antiparticle decay chain, where π_s^+ refers to a low-momentum ("slow") pion accompanying the D^0.

Charged tracks measured by the CTD and assigned to the primary event vertex[3] were selected. The transverse momentum was required to be greater than $0.12\,\mathrm{GeV}$. The p_T cut was raised to $0.25\,\mathrm{GeV}$ for a data subsample corresponding to $(16.9 \pm 0.4)\,\mathrm{pb}^{-1}$, for which the low-momentum track-reconstruction efficiency was lower due to the operating conditions of the CTD [19]. Each track was required to reach at least the third superlayer of the CTD. These restrictions ensured that the track acceptance was high and the momentum resolution was good. Tracks in the CTD with opposite charges and transverse momenta $p_T > 0.45\,\mathrm{GeV}$ were combined in pairs to form D^0 candidates. The tracks were alternately assigned the kaon and the pion mass and the invariant mass of the pair, $M_{K\pi}$, was determined. Each additional track, with charge opposite to that of the kaon track, was assigned the pion mass and combined with the D^0-meson candidate to form a D^* candidate.

A mass window for the signal region of the D^0 varying from $1.82 < M_{K\pi} < 1.91\,\mathrm{GeV}$ to $1.79 < M_{K\pi} < 1.94\,\mathrm{GeV}$ was used, reflecting the dependence of the CTD resolution on $p_T(D^*)$. The signal region for the reconstructed mass difference $\Delta M = (M_{K\pi\pi_s} - M_{K\pi})$ was $0.1435 < \Delta M < 0.1475\,\mathrm{GeV}$. The requirement of $p_T(D^*)/E_T^{\theta > 10^\circ} > 0.1$ was also applied, where $E_T^{\theta > 10^\circ}$ is the transverse energy outside a cone of $\theta = 10^\circ$ defined with respect to the proton direction. This cut rejects background without significantly affecting the signal.

---

[3] The resolution of such tracks is not good enough to separate primary and secondary vertices from c and b hadron decays.

The D^* mesons were selected in the kinematic region $1.5 < p_T(D^*) < 9$ GeV and $|\eta(D^*)| < 1.5$. The ΔM distribution for events with an electron reconstructed in the BPC is shown in Fig. 1. To extract the number of D^* mesons, the ΔM distribution was fit using an unbinned likelihood method, with a Gaussian to describe the signal and a threshold function to describe the combinatorial background. A first estimate of the background was given by D^* candidates with wrong-sign combinations, in which both tracks forming the D^0 candidates have the same charge and the third track has the opposite charge. These are shown as the shaded region in Fig. 1. The number of D^* mesons obtained from the fit was $N(D^*) = 253 \pm 25$.

5 Acceptance corrections and systematic uncertainties

The acceptances were calculated using the HERWIG 6.1 [20] and RAPGAP 2.08 [21] Monte Carlo (MC) models. Both models simulate charm and beauty production and include contributions from both direct and resolved photoproduction. In direct photoproduction the photon participates as a point-like particle in the hard scattering process, while in resolved photoproduction a parton in the photon scatters on a parton in the proton. The generated events were passed through a full simulation of the detector, using GEANT 3.13 [22] and then processed and selected with the same programs as used for the data. The CTEQ5L [23] parton density function (PDF) was used for the proton and GRV-LO [24] was used for the photon. The charm-quark mass was set to 1.5 GeV.

The HERWIG predictions are in good agreement with the data distributions for both the scattered lepton and hadronic variables and so this Monte Carlo was used to correct the data for detector effects. For the kinematic region of the measurement $0.05 < Q^2 < 0.7$ GeV^2, $0.02 < y < 0.85$, $1.5 < p_T(D^*) < 9$ GeV, and $|\eta(D^*)| < 1.5$ the acceptance was $(1.11 \pm 0.03)\%$. This includes the geometrical acceptance of the BPC, which was about 9%, and the reconstruction efficiency for the D^* decay chain.

The RAPGAP MC gives a similarly good representation of the data and was used to estimate part of the systematic uncertainties, as described below.

The differential cross section for a given observable Y was determined using

$$\frac{d\sigma}{dY} = \frac{N}{A \cdot \mathcal{L} \cdot B \cdot \Delta Y},$$

where N is the number of D^* events in a bin of size ΔY, A is the acceptance (which takes into account migrations and efficiencies for that bin) and $\mathcal{L}$ is the integrated luminosity.

The product, B, of the appropriate branching ratios for the D^* and D^0 decays was set to $(2.57 \pm 0.05)\%$ [25].

The systematic uncertainties of the measured cross sections were determined by changing in turn the selection cuts or the analysis procedure within their uncertainties and repeating the extraction of the cross sections [26]. The major experimental sources of systematic uncertainty were (the variation of the total cross section is given in parentheses): the BPC alignment ($^{+2.5}_{-3.1}\%$) and energy scale ($^{+0.4}_{-1.2}\%$); the uncertainty in the CTD momentum scale ($^{+0.2}_{-1.5}\%$) and the CAL energy scale ($\pm 1\%$); the $p_T(D^*)/E_T^{\theta>10°}$ cut ($^{+3.0}_{-1.7}\%$) and the D^* signal extraction ($^{+0.1}_{-1.5}\%$). The uncertainty due to the MC model ($^{+9.5}_{-4.8}\%$) was determined by using RAPGAP to evaluate the acceptance correction rather than HERWIG, as well as by varying the fraction of resolved and direct photoproduction processes in the simulation.

All the above errors were added in quadrature separately for the positive and negative variations to determine the overall systematic uncertainty. The overall normalisation has additional uncertainties of 2.2% due to the luminosity measurement and 2.0% due to knowledge of branching ratios. These are included in the error quoted for the total cross section but not in the systematic uncertainties of the differential cross sections.

6 Theoretical predictions

Two different calculations were used to evaluate the theoretical expectation for charm production.

The HVQDIS program [27] implements an NLO calculation of charm production in DIS. At low Q^2, the hadron-like structure of the photon, not included in HVQDIS, is needed to regularise the NLO calculation. Therefore predictions from this program are expected to lose accuracy in the limit $Q^2 \to 0$. The ZEUS measurements of D^* production in DIS for $Q^2 > 1.5\,\mathrm{GeV}^2$ are in good agreement with the HVQDIS prediction [5].

The FMNR program [28] implements an NLO calculation of charm photoproduction which includes the hadron-like component of the photon. Electroproduction cross sections can be obtained with FMNR using the Weizsäcker-Williams approximation [29] and are therefore expected to be reliable only at low Q^2, where this approximation is valid. The FMNR predictions are in reasonable agreement with ZEUS measurements of D^* photoproduction [7], considering the theoretical uncertainties.

It is therefore interesting to see whether these calculations are able to reproduce the data in the transition region between photoproduction and DIS. The following parameters were used in the calculations for both programs. They were chosen to be the same as in a previous publication [5]. A variant of the ZEUS-S NLO QCD global fit [30] to

structure-function data was used as the parameterisation of the proton PDFs. This fit was repeated in the fixed-flavour-number scheme, FFNS, in which the PDF has three active quark flavours in the proton, and $\Lambda_{\text{QCD}}^{(3)}$ is set to $0.363\,\text{GeV}$. The mass of the charm quark was set to $1.35\,\text{GeV}$. The renormalisation and factorisation scales were set to $\mu_R = \mu_F = \sqrt{Q^2 + 4m_c^2}$ in HVQDIS, while for FMNR they were set to the usual choice of $\mu_R = \mu_F = \sqrt{p_T^2 + m_c^2}$, where p_T^2 is the average transverse momentum squared of the charm quarks. The charm fragmentation to a D^* is carried out using the Peterson function [31]. The hadronisation fraction, $f(c \to D^*)$, was taken to be 0.238 [32] and the Peterson parameter, ϵ, was set to 0.035 [33]. The parameters used here for the FMNR calculation are different from those used in a previous photoproduction analysis [7] (which used $m_c = 1.5\,\text{GeV}$) leading to a 20% larger predicted photoproduction cross section.

For the FMNR calculation the electroproduction cross section, σ_{ep}, was obtained from the photoproduction cross section, $\sigma_{\gamma p}(W)$, using

$$\sigma_{ep} = \int\limits_{y_{\text{min}}}^{y_{\text{max}}} dy\,\Phi(y, Q_{\text{min}}^2, Q_{\text{max}}^2)\sigma_{\gamma p}(\sqrt{ys}),$$

where

$$\Phi(y, Q_{\text{min}}^2, Q_{\text{max}}^2) = \frac{\alpha_{\text{em}}}{2\pi}\left[\frac{(1 + (1-y)^2)}{y}\ln\frac{Q_{\text{max}}^2}{Q_{\text{min}}^2} - 2m_e y\left(\frac{1}{Q_{\text{min}}^2} - \frac{1}{Q_{\text{max}}^2}\right)\right] \quad (1)$$

is the photon flux and y_{min}, y_{max}, Q_{min}^2, Q_{max}^2 define the measurement range in y and Q^2.

The NLO QCD predictions for D^* production are affected by systematic uncertainties, which were also evaluated as in a previous ZEUS paper [5][4]. The sources of systematic uncertainties on the total cross section are: charm quark mass ($^{+15}_{-13}\%$ for HVQDIS, $^{+16}_{-14}\%$ for FMNR); renormalisation and factorisation scale ($^{+1}_{-13}\%$ for HVQDIS, $^{+23}_{-10}\%$ for FMNR); ZEUS PDF ($\pm 5\%$); fragmentation ($^{+10}_{-6}\%$). For both programs, the systematic uncertainties were added in quadrature and are displayed as a band in the figures.

Theoretical calculations of the total charm cross section in this Q^2 range can not be compared to the present data since D^* are only measured in a limited p_T and η range.

7   Cross section measurements

The total cross section for $0.05 < Q^2 < 0.7\,\text{GeV}^2$, $0.02 < y < 0.85$, $1.5 < p_T(D^*) < 9\,\text{GeV}$ and $|\eta(D^*)| < 1.5$ is:

$$\sigma(ep \to eD^*X) = 10.1 \pm 1.0(\text{stat.})^{+1.1}_{-0.8}(\text{syst.}) \pm 0.20(\text{BR})\,\text{nb},$$

---

[4] For the HVQDIS case, following [5], the minimum value for the scales was set to $2m_c$.

6

where the first uncertainty is statistical, the second from systematic effects (including the luminosity uncertainty) and the third from the uncertainties in the branching ratios.

The prediction from the HVQDIS program is $8.6^{+1.9}_{-1.8}$ nb, in agreement with the data, while the prediction from FMNR is $8.9^{+2.4}_{-1.4}$ nb[5], also in good agreement.

The measured differential D^* cross sections as a function of Q^2, y, $p_T(D^*)$ and $\eta(D^*)$ for the data are shown in Fig. 2 and given in Table 1. The predictions of the NLO calculations, including their uncertainties, are shown as bands. The measured differential cross sections are well described over the full measured kinematic region by both calculations.

This analysis was also compared to previous ZEUS measurements of D^* production in DIS [5] made in the kinematic region $1.5 < Q^2 < 1000\,\text{GeV}^2$, $0.02 < y < 0.7$, $1.5 < p_T(D^*) < 15\,\text{GeV}$ and $|\eta(D^*)| < 1.5$. In order to directly compare with the results presented there, the cross sections were recalculated in the modified kinematic region $0.02 < y < 0.7$. No correction was made for the different upper cut on $p_T(D^*)$, as the size of the effect is $\approx 1\%$.

For this modified kinematic region, the differential cross section as a function of Q^2 is presented in Fig. 3 and given in Table 2. The systematic errors were assumed to be the same as those in the full y range. Figure 3 also shows the previous ZEUS measurement and the HVQDIS prediction. The combination of both measurements shows that the slope of $d\sigma/dQ^2$ changes with Q^2; at high Q^2 the slope is steeper than at low Q^2. The NLO calculation describes the measured data well over the full Q^2 range.

The D^* electroproduction cross sections were converted to γp cross sections, $\sigma_{\gamma p}$, in the range $1.5 < p_T(D^*) < 9\,\text{GeV}$ and $|\eta(D^*)| < 1.5$ (measured in the laboratory frame) using the photon flux from Eq. 1. The cross sections are given for $W = 160\,\text{GeV}$, which corresponds to $y = 0.25$, close to the mean y of the measured cross sections. The W dependence of $\sigma_{\gamma p}$ was evaluated from the data. The uncertainty of this procedure was estimated to be 10%. A comparison of the charm photoproduction cross section [7], this measurement and the DIS cross sections [5] is shown in Fig. 4. The numbers are tabulated in Table 3. The photoproduction point was corrected for the different kinematic range and centre-of-mass energy used here using the FMNR program. As can be seen, the present measurements are consistent with the photoproduction cross section. A fit using a function of the form $\sigma(Q^2) = SM^2/(Q^2 + M^2)$, where S is the photoproduction cross section at $Q^2 = 0$ and M^2 is the scale at which the γp cross section changes from the photoproduction value to the DIS $1/Q^2$ behaviour, gives a good description of the data over the whole Q^2 range with $S = 823 \pm 63$ nb and $M^2 = 13 \pm 2\,\text{GeV}^2$. The value of M^2 found here for charm production is close to $4m_c^2$ [34] and significantly larger than that found for inclusive data $M_0^2 = 0.52 \pm 0.05\,\text{GeV}^2$ [12].

---

[5] The contribution from the hadron-like component of the photon is 9%.

8 Conclusions

Charm production has been measured as a function of Q^2, y, $p_T(D^*)$ and $\eta(D^*)$ in the kinematic region $0.05 < Q^2 < 0.7\,\mathrm{GeV}^2$, $0.02 < y < 0.85$, $1.5 < p_T(D^*) < 9.0\,\mathrm{GeV}$ and $|\eta(D^*)| < 1.5$. These measurements extend the previous ZEUS measurements in DIS to lower Q^2. The measured differential cross sections are well described by two different NLO QCD calculations: one (FMNR) is designed for the photoproduction region; while the other (HVQDIS) is designed for DIS. Both calculations predict similar cross sections in the intermediate Q^2 region measured here, which agree well with the measurements. The measurements, converted to γp cross sections, also agree well with the D^* photoproduction data.

Acknowledgements

References

[1] ZEUS Collaboration, J. Breitweg et al., Phys. Lett. B 407 (1997) 402.

[2] H1 Collaboration, C. Adloff et al., Nucl. Phys. B 545 (1999) 21.

[3] ZEUS Collaboration, J. Breitweg et al., Eur. Phys. J. C 12 (2000) 35.

[4] H1 Collaboration, C. Adloff et al., Phys. Lett. B 528 (2002) 199.

[5] ZEUS Collaboration, S. Chekanov et al., Phys. Rev. D 69 (2004) 012004.

[6] H1 Collaboration, S. Aid et al., Nucl. Phys. B 472 (1996) 32.

[7] ZEUS Collaboration, J. Breitweg et al., Eur. Phys. J. C 6 (1999) 67.

[8] ZEUS Collaboration, S. Chekanov et al., Nucl. Phys. B 729 (2005) 492.

[9] H1 Collaboration, A. Aktas et al., Eur. Phys. J. C 47 (2006) 597.

[10] H1 Collaboration, A. Aktas et al., Preprint hep-ex/0608042, 2006. Submitted to Eur. Phys. J. C.

[11] ZEUS Collaboration, J. Breitweg et al., Phys. Lett. B 407 (1997) 432.

[12] ZEUS Collaboration, J. Breitweg et al., Phys. Lett. B 487 (2000) 53.

[13] ZEUS Collaboration, U. Holm (ed.), *The ZEUS Detector*. Status Report (unpublished), DESY (1993), available on
`http://www-zeus.desy.de/bluebook/bluebook.html`.

[14] N. Harnew et al., Nucl. Inst. Meth. A 279 (1989) 290;
B. Foster et al., Nucl. Phys. Proc. Suppl. B 32 (1993) 181;
B. Foster et al., Nucl. Inst. Meth. A 338 (1994) 254.

[15] M. Derrick et al., Nucl. Inst. Meth. A 309 (1991) 77;
A. Andresen et al., Nucl. Inst. Meth. A 309 (1991) 101;
A. Caldwell et al., Nucl. Inst. Meth. A 321 (1992) 356;
A. Bernstein et al., Nucl. Inst. Meth. A 336 (1993) 23.

[16] J. Andruszków et al., Preprint DESY-92-066, DESY, 1992;
ZEUS Collaboration, M. Derrick et al., Z. Phys. C 63 (1994) 391;
J. Andruszków et al., Acta Phys. Pol. B 32 (2001) 2025.

[17] W.H. Smith, K. Tokushuku and L.W. Wiggers,. Proc. Computing in High-Energy Physics (CHEP), C. Verkerk and W. Wojcik (eds.), p. 222. Annecy, France, CERN (1992). Also in preprint DESY 92-150B, 1992.

[18] J. Tandler. Ph.D. Thesis, Universität Bonn, Bonn, Germany, Report BONN-IR-2003-06 (unpublished), (2003), available on
`http://www-zeus.physik.uni-bonn.de/german/phd.html`.

[19] D.S. Bailey and R. Hall-Wilton, Nucl. Inst. Meth. A 515 (2003) 37.

[20] G. Marchesini et al., Preprint Cavendish-HEP-99/17 (hep-ph/9912396), 1999;
G. Marchesini et al., Comp. Phys. Comm. 67 (1992) 465.

[21] H. Jung, Comp. Phys. Comm. 86 (1995) 147.

[22] R. Brun et al., GEANT3, Technical Report CERN-DD/EE/84-1, CERN, 1987.

[23] CTEQ Collaboration, H.L. Lai et al., Eur. Phys. J. C 12 (2000) 375.

[24] M. Glück, E. Reya and A. Vogt, Phys. Rev. D 46 (1992) 1973.

[25] Particle Data Group, W.-M. Yao et al., J. Phys G 33 (2006) 1.

[26] P. Irrgang. Ph.D. Thesis, Universität Bonn, Bonn, Germany, Report
BONN-IR-2004-016 (unpublished), (2004), available on
http://www-zeus.physik.uni-bonn.de/german/phd.html.

[27] B.W. Harris and J. Smith, Phys. Rev. D 57 (1998) 2806.

[28] S. Frixione, P. Nason and G. Ridolfi, Nucl. Phys. B 454 (1995).

[29] S. Frixione et al., Phys. Lett. B 319 (1993) 339.

[30] ZEUS Collaboration, S. Chekanov et al., Phys. Rev. D 67 (2003) 012007.

[31] C. Peterson et al., Phys. Rev. D 27 (1983) 105.

[32] L. Gladilin, Preprint hep-ex/9912064, 1999;
ZEUS Collaboration, S. Chekanov et al., Eur. Phys. J. C 44 (2005) 351.

[33] P. Nason and C. Oleari, Nucl. Phys. B 565 (2000) 245.

[34] V.M. Budnev et al., Phys. Rep. 15C (1974) 181.

Q^2 bin (GeV^2)	$d\sigma/dQ^2$ (nb/ GeV^2)	Δ_{stat}	Δ_{syst}
0.05:0.20	29.1	± 7.2	$^{+4.3}_{-4.1}$
0.20:0.35	15.0	± 2.4	$^{+1.5}_{-1.4}$
0.35:0.50	10.7	± 2.2	$^{+1.3}_{-1.1}$
0.50:0.70	7.1	± 2.3	$^{+1.6}_{-0.8}$
y bin	$d\sigma/dy$ (nb)	Δ_{stat}	Δ_{syst}
0.02:0.15	34.2	± 6.7	$^{+7.5}_{-7.5}$
0.15:0.30	19.5	± 3.8	$^{+2.7}_{-2.1}$
0.30:0.50	10.7	± 2.1	$^{+1.2}_{-1.1}$
0.50:0.85	3.8	± 1.1	$^{+0.8}_{-0.8}$
$p_T(D^*)$ bin (GeV)	$d\sigma/dp_T(D^*)$ (nb/ GeV)	Δ_{stat}	Δ_{syst}
1.5:2.5	6.8	± 1.7	$^{+1.0}_{-0.9}$
2.5:3.8	2.2	± 0.3	$^{+0.2}_{-0.2}$
3.8:5.0	0.53	± 0.11	$^{+0.02}_{-0.02}$
5.0:9.0	0.11	± 0.02	$^{+0.01}_{-0.01}$
$\eta(D^*)$ bin	$d\sigma/d\eta(D^*)$ (nb)	Δ_{stat}	Δ_{syst}
-1.5: -0.5	3.4	± 0.6	$^{+0.7}_{-0.7}$
-0.5: 0.0	4.1	± 0.9	$^{+0.5}_{-0.4}$
0.0: 0.5	2.9	± 0.8	$^{+0.3}_{-0.3}$
0.5: 1.5	3.3	± 0.7	$^{+0.4}_{-0.3}$

Table 1: *Measured differential cross sections as a function of Q^2, y, $p_T(D^*)$ and $\eta(D^*)$ for $0.05 < Q^2 < 0.7$ GeV^2, $0.02 < y < 0.85$, $1.5 < p_T(D^*) < 9$ GeV and $|\eta(D^*)| < 1.5$. The statistical and systematic uncertainties are shown separately. The normalisation uncertainties from the luminosity measurement and the branching ratios are not included in the systematic uncertainties.*

11

Q^2 bin	$d\sigma/dQ^2$	Δ_{stat}
(GeV^2)	(nb/ GeV^2)	
0.05:0.20	30.0	± 7.2
0.20:0.35	14.0	± 2.3
0.35:0.50	10.3	± 2.1
0.50:0.70	6.9	± 2.3

Table 2: *Measured differential cross sections as a function of Q^2 for $0.02 < y < 0.7$, $1.5 < p_T(D^*) < 9$ GeV and $|\eta(D^*)| < 1.5$. The systematic uncertainties are assumed to be the same as those for the kinematic range $0.02 < y < 0.85$.*

Q^2 (GeV^2)	$\sigma_{\gamma p}$	Δ_{stat} (nb)	Δ_{syst}
~ 0	729	± 46	$^{+110}_{-92}$
0.10	710	± 170	$^{+200}_{-200}$
0.26	810	± 130	$^{+180}_{-180}$
0.42	940	± 200	$^{+260}_{-260}$
0.59	890	± 290	$^{+370}_{-360}$
2.7	741	± 31	$^{+95}_{-100}$
7.1	506	± 27	$^{+81}_{-59}$
14	408	± 22	$^{+64}_{-47}$
28	278	± 13	$^{+36}_{-33}$
57	152	± 13	$^{+24}_{-24}$
130	64	± 9	$^{+14}_{-11}$
450	21	± 5	$^{+6}_{-11}$

Table 3: γp cross sections for D^* production in the range $1.5 < p_T(D^*) < 9$ GeV and $|\eta(D^*)| < 1.5$ as a function of Q^2 for $W = 160$ GeV. The values at $Q^2 \approx 0$ and for $Q^2 > 2.7$ GeV^2 are obtained from previous photoproduction [7] and DIS measurements [5] in the range $1.5 < p_T(D^*) < 15$ GeV and $|\eta(D^*)| < 1.5$.
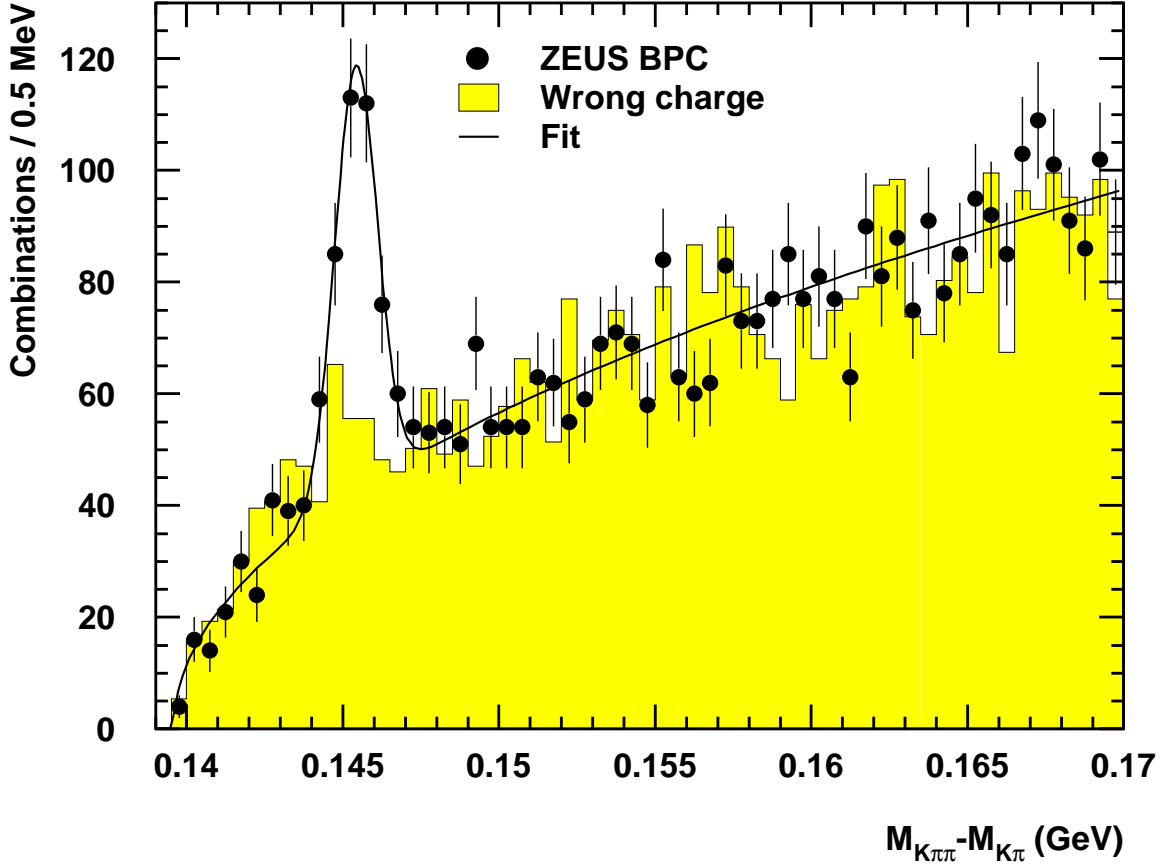
Figure 1: *The distribution of the mass difference, $\Delta M = M(K\pi\pi_s) - M(K\pi)$, for $D^{*\pm}$ candidates with a measured scattered electron in the BPC. The histogram shows the ΔM distribution for wrong charge combinations, normalised to the data in the region $0.151 < \Delta M < 0.167$. The normalisation factor is 1.07. The solid curve is the result of the fit described in the text.*
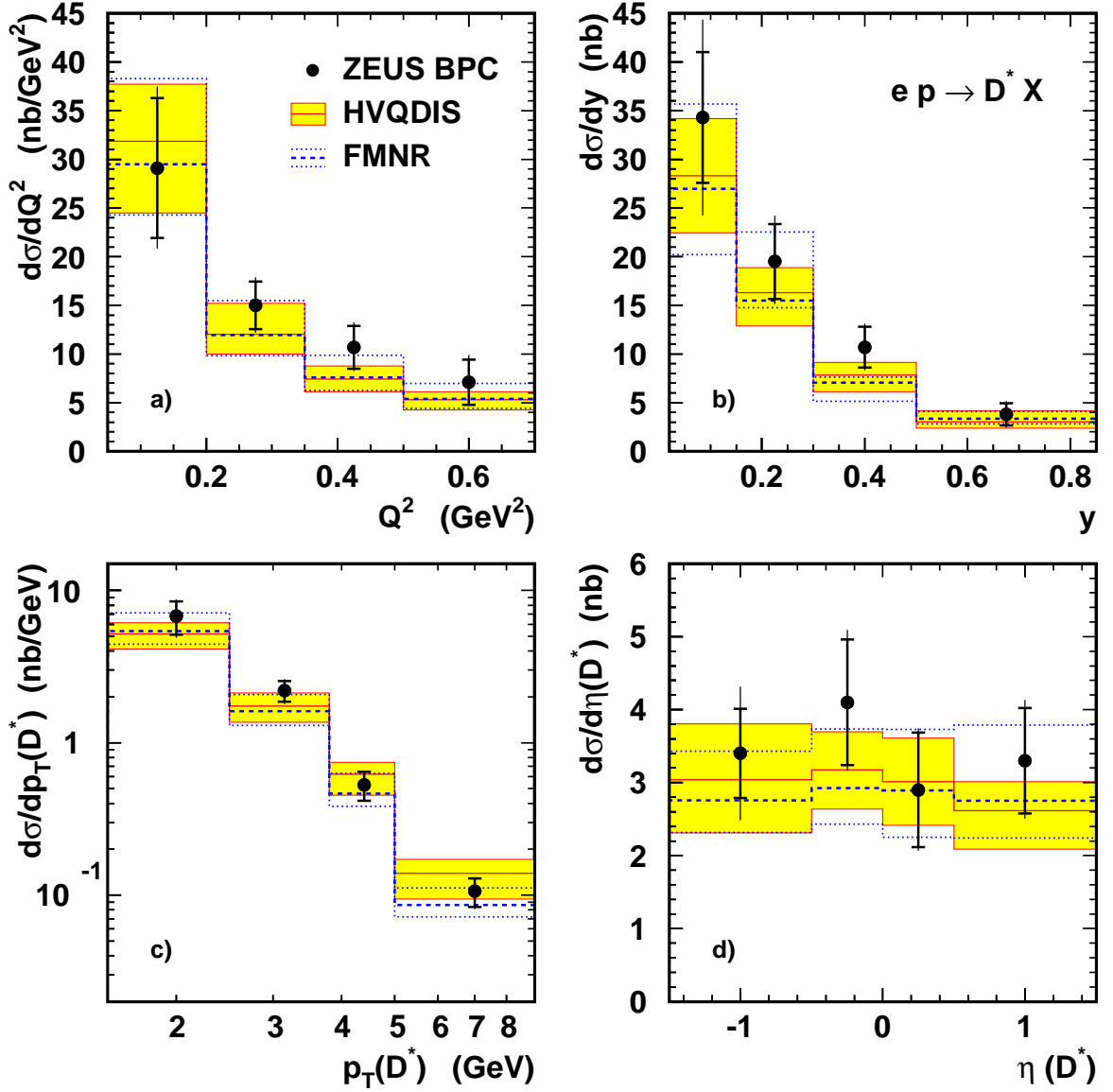
ZEUS

Figure 2: *Differential D^* production cross sections as a function of (a) Q^2, (b) y, (c) $p_T(D^*)$ and (d) $\eta(D^*)$ compared to the HVQDIS and FMNR NLO predictions. Data are represented by points. The inner error bars are the statistical errors of the measurement while the open error bars are the sum of statistical and systematic uncertainties added in quadrature. The shaded area indicates the theoretical uncertainties obtained by variation of the HVQDIS parameters. The dashed and dotted lines represent the central value of the FMNR calculation and its uncertainty, respectively.*
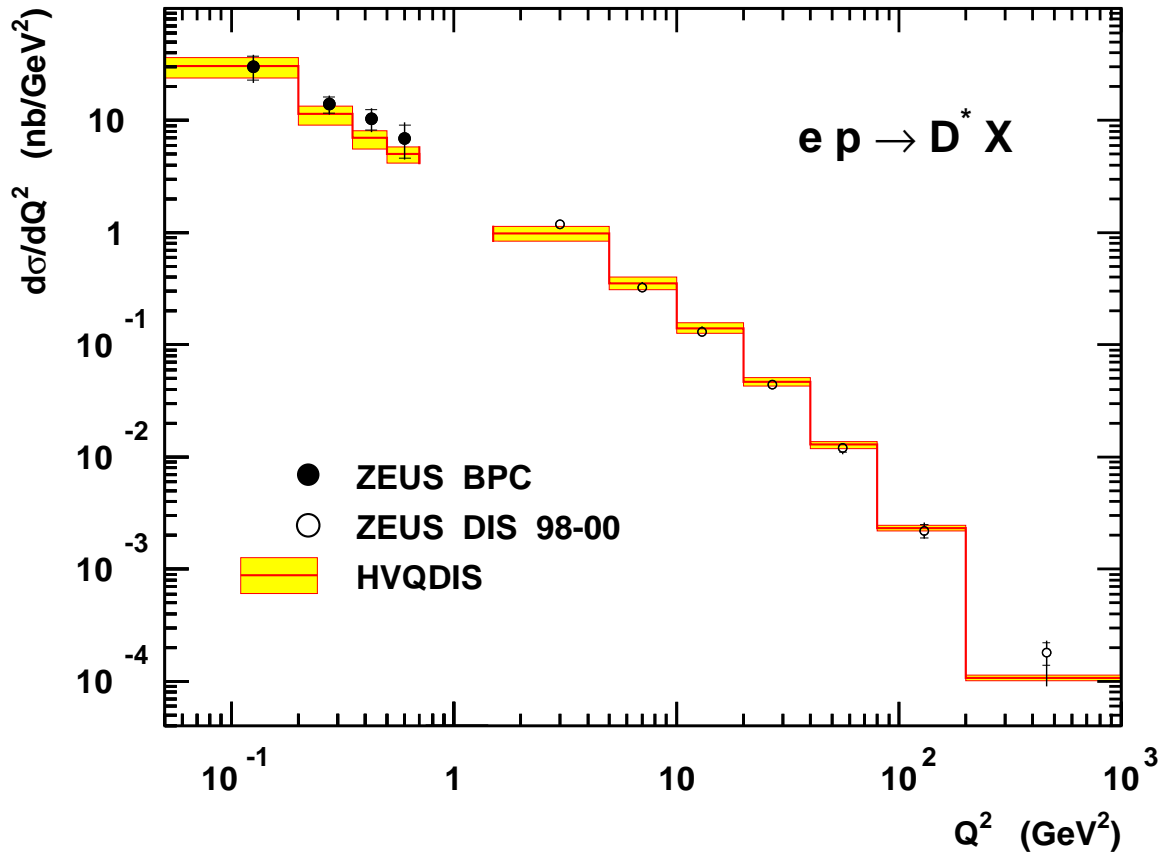
Figure 3: *The D^* production cross section as a function of Q^2 in the kinematic region $0.02 < y < 0.7$, $1.5 < p_T(D^*) < 9\,GeV$ and $|\eta(D^*)| < 1.5$ for this measurement (BPC) and previous results on D^* production in DIS [5] (for $1.5 < p_T(D^*) < 15\,GeV$), compared to the HVQDIS NLO prediction. The data are represented by points. The inner error bars are statistical while the open error bars are the sum of statistical and systematic uncertainties added in quadrature. The shaded area indicates the theoretical uncertainties obtained by variations of the HVQDIS parameters.*
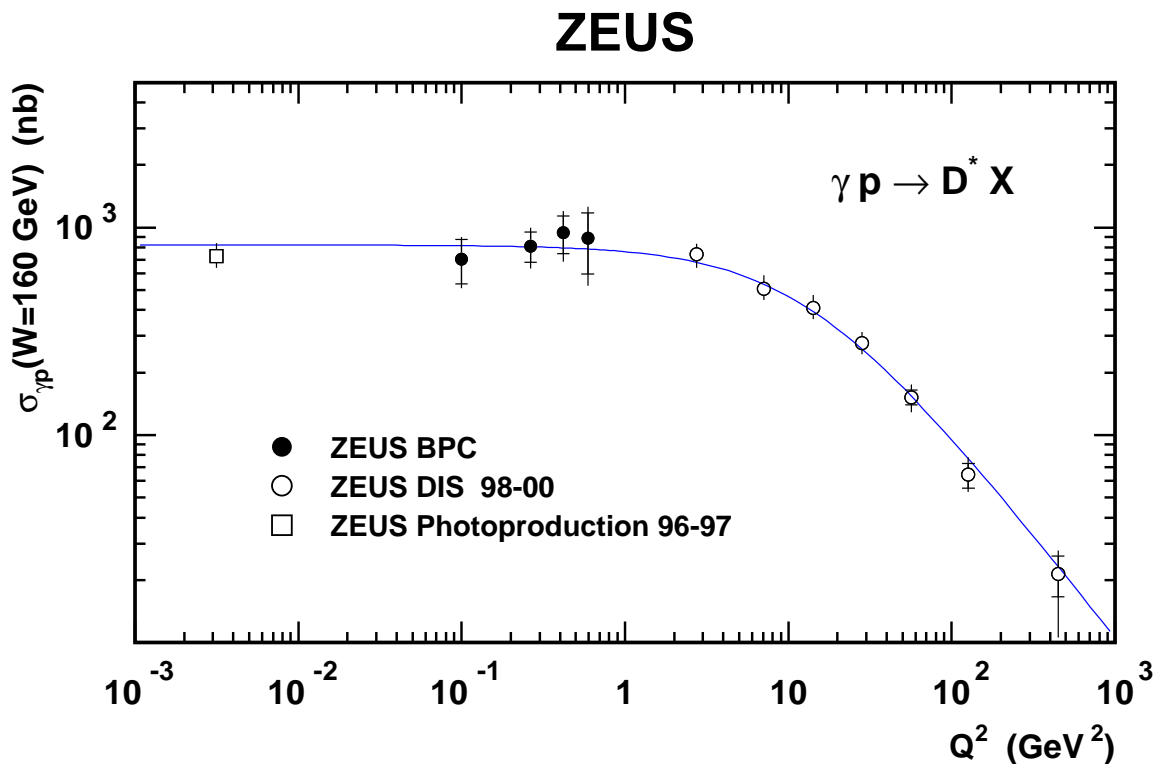
ZEUS

$\gamma\,\mathbf{p} \to \mathbf{D}^* \mathbf{X}$

- ● ZEUS BPC
- ○ ZEUS DIS 98-00
- □ ZEUS Photoproduction 96-97

Figure 4: *The γp cross section for $D^{*\pm}$ production in the range $1.5 < p_T(D^*) < 9\ GeV$ and $|\eta(D^*)| < 1.5$ as a function of Q^2 from this paper (BPC), compared with previous results on D^* production in DIS [5] and photoproduction [7] for $1.5 < p_T(D^*) < 15\ GeV$ and $|\eta(D^*)| < 1.5$. The data are represented by points. The inner error bars are statistical while the open error bars are the sum of statistical and systematic uncertainties added in quadrature. The photoproduction point is drawn at $Q^2 = 0.003\ GeV^2$ for convenience. The curve shows a fit to the data described in the text.*